

pH dependence of charge multipole moments in proteins

Anže Lošdorfer Božič^{1,*} and Rudolf Podgornik^{1,2}

¹*Department of Theoretical Physics, Jožef Stefan Institute, SI-1000 Ljubljana, Slovenia*

²*Department of Physics, Faculty of Mathematics and Physics,*

University of Ljubljana, SI-1000 Ljubljana, Slovenia

(Dated: April 12, 2022)

Electrostatic interactions play an important role in the structure and function of proteins. Due to ionizable amino acid residues present on the solvent-exposed surfaces of proteins, the charge on the proteins is not constant but varies with the changes in their environment – most notably, the pH of the surrounding solution. We study the effects of pH on the charge of four globular proteins by expanding their surface charge distributions in terms of multipoles. The detailed representation of the charges on the proteins is in this way replaced by the *magnitudes* and *orientations* of the multipole moments of varying order. Focusing on the three lowest-order multipoles – the total charge, dipole, and quadrupole moment – we show that the value of pH influences not only their magnitudes, but more notably also the spatial orientation of their principal axes. Our findings could have important consequences for the study of protein-protein interactions and the assembly of both proteinaceous shells and patchy colloids with dissociable charge groups.

arXiv:1703.09948v1 [physics.bio-ph] 29 Mar 2017

* anze.bozic@ijs.si; Corresponding author

INTRODUCTION

Electrostatic interactions are an important part of the long- and short-range interactions in the biological environment. They can be mostly understood within the framework of the generalized DLVO (Derjaguin-Landau-Verwey-Overbeek) theory of interactions between colloids, where the canonical electrostatic and van der Waals components are supplemented by the solvent structure effects of either hydration or hydrophobic type [1]. This general decomposition of the interactions remains valid also for proteins in aqueous solution, where it is in addition augmented by short-range recognition and docking interactions as well as specific ion effects [2, 3].

Just as the van der Waals interactions are a functional of the dielectric response function [4, 5], so are the electrostatic interactions within and between the proteins defined by their charge distributions. The charge distributions and the consequent electrostatic interactions that dominate many aspects of the protein behavior can be modelled on different levels of detail [6–8]. One of the defining differences between the electrostatics of proteins and the generic electrostatics of colloids that needs to be taken into account is the existence of *ionizable amino acid residues* in proteins. The interactions and energetics of these residues enable local charge separation and thus determine the distribution of charge in proteins [7, 9] and consequently the electrostatic protein-protein interactions [10–12]. The mechanism of charge separation in turn creates a distinction between the undissociated chargeable groups buried inside the proteins on the one hand and the solvent-exposed and dissociable surface charges on the other [13]. This distinction can be blurred, as internal ionizable groups can be to some extent dielectrically shielded even in the strongly hydrophobic protein core [14, 15].

Identification of the dissociable, solvent-exposed amino acid residues is the first step in obtaining the description of charge distributions in proteins. Afterwards, one needs to take into account the proper description of the dissociation mechanism for the deprotonated carboxylate of aspartic and glutamic acid, deprotonated hydroxyl of the tyrosine phenyl group, the protonated amine group of arginine and lysine, and the protonated secondary amine of histidine [8, 16]. Since the dissociation process and the local electrostatic field are coupled via the charge regulation mechanism [17], the dissociation rate depends on the local pH that can be obtained only self-consistently [18, 19]. In principle, only detailed *ab initio* simulations can provide a detailed quantification of the partial charges buried inside or exposed on a protein surface. These simulations are, however, usually hampered by the sheer size and number of atoms one needs to invoke in order to achieve a necessary amount of realism for the calculations [20–22].

A proper quantification of the electrostatic interactions in proteins requires the encoding of not only the magnitudes of the charges but also of their distribution in space [23, 24]. The latter can be represented to any desirable accuracy by a multipole expansion of the charge density, where each term in the multipole series describes a deviation with a specific symmetry from the zeroth-order, spherically symmetric distribution [25]. There are many variants of the multipole expansion, done either on the level of amino acids or on the level of complete proteins [26–28], with the most straightforward being the *irreducible spherical representation* of the multipoles [23]. This representation is obtained by mapping the charge distribution on the original solvent-accessible protein surface onto a sphere circumscribed to the protein [24, 29, 30].

The multipole expansion provides a bridge between a coarse-grained description of the charge density and its detailed microscopic description, the level of detail depending on the multipole order of the expansion used. As such, even multipoles of lower order can provide a *signature* of charge distributions in molecules [23, 31–33], and a small number of higher-order multipoles can account for almost all of the electrostatic field in the aqueous solvent [24]. In the presence of ionic screening this otherwise standard result is modified, as the effects of charge anisotropy and higher-order multipole moments then extend to the far-field region. In contrast to the standard multipole expansion, the screened electrostatic potential retains the full directional dependence of all multipole moments, an important difference which is often overlooked [34–37].

With a few exceptions [24], the pH dependence of charge distributions in proteins has been studied mostly on the level of the spherically symmetric total charge, that is, the zeroth multipole moment. For higher-order multipoles, however, the two components of the multipole expansion – the magnitude of the multipole moments and their spatial distribution – can hardly be separated. Our work aims at investigating not only the pH dependence of the *magnitudes* but also of the *directions of the principal axes* of the charge dipole and quadrupole moments in proteins. It is in fact the latter dependencies that are of particular importance for the local electrostatic interactions either in an ordered protein assembly (such as a proteinaceous virus shell [38]), between charged Janus colloids [39], or indeed in the general context of patchy globular proteins, colloids, and polyelectrolytes [40–45]. The changes in the orientation of multipole moment axes could also be driving local packing symmetry transitions, tailgating the imposed changes in pH and bathing salt concentration.

MATERIALS AND METHODS

Protein data

For our study we chose four protein structures from the RCSB Protein Data Bank (PDB) [46]: hen egg-white lysozyme (2lyz), human serum albumin (1e7h), bovine β -lactoglobulin (2blg), and phage MS2 capsid protein (2ms2, subunit A). They have globular geometry, easily approximated by a sphere, and most of them are fairly small, with lysozyme and MS2 capsid protein being composed of 129 amino acids (AA), and β -lactoglobulin of 162 AA. Human serum albumin (HSA) is the largest of the four, consisting of 585 AA.

To obtain the surface charges on each protein at a given pH value, we first determine which AA residues are solvent-accessible, and compute the charge on them by using the canonical static dissociation constant pK_a value pertaining to each AA type. By projecting the positions of the charged residues onto a sphere, we obtain the surface charge distribution of each protein, which we then use to compute the electrostatic multipole moments. Details of each of these steps are laid out in the following Subsections, and a sketch of the model is shown in Fig. 1.

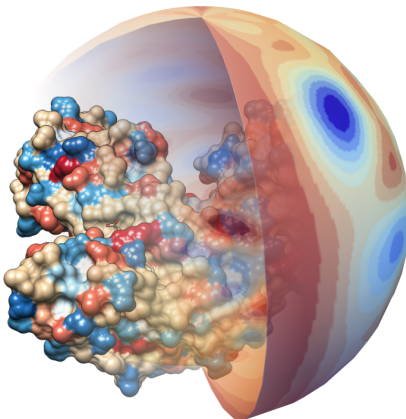


Figure 1. Sketch of our model showing a rendering of the surface structure of human serum albumin (1e7h), superimposed onto a circumscribed sphere with projected multipole expansion of the surface charge distribution (up to $\ell_{\max} = 12$). AA residues that are charged at $pH = 7$ are highlighted in the structure, with colors pertaining to the red spectrum indicating positive charges, and colors in the blue spectrum indicating negative charges. The same color scheme applies to the projection of the charge distribution onto the sphere. The protein structure was rendered with UCSF Chimera [47].

Relative solvent accessibility of amino acid residues

The relative solvent accessibility (RSA) of an amino acid indicates its degree of burial in the three-dimensional protein structure, and is important in determining which AA residues can contribute to the surface charge of the protein. We obtain the RSA of each AA in a protein with the help of the UCSF Chimera software [47, 48] by normalizing the solvent-exposed surface area of each residue in the protein structure with the surface area of the same type of residue in a reference state [49]. The classification of AA residues as “buried” or “exposed” is then done on the basis of an RSA cut-off c , which typically ranges between 5% and 30% [50–53]. We opt for a cut-off of $c = 0.25$, thus defining as *exposed* all amino acid residues AA_k with an RSA value greater than 25%:

$$\text{RSA}(AA_k) \geq 0.25 \Rightarrow AA_k \in \text{exposed}. \quad (1)$$

The choice of this (arbitrary) cut-off influences the number of charged residues that will be taken into account in our calculation of the surface charge of the protein. How the number of charges varies with the selection of the RSA cut-off is shown in Table S1 in the Supplementary Material. Similar variations in the number of surface charges could also occur, for instance, due to a different choice of the normalization values (reference states) in the calculation of the RSA [54].

For consistency, we use the RSA cut-off of $c = 0.25$ throughout the paper, unless specified otherwise. However, we also test our predictions for several other values of the cut-off and show that it bears no influence on the conclusions obtained in our work.

pH dependence of charged amino acid residues

Once we know which AAs are exposed to the solvent and thus dissociable, we can determine their charge at a given pH value. The charged residues we consider are the aspartic acid (ASP), glutamic acid (GLU), tyrosine (TYR), cysteine (CYS), arginine (ARG), lysine (LYS), and histidine (HIS). To obtain the charge on each of the residues as a function of pH we use the acid-base dissociation constants pK_a from Ref. [55] (and listed in Table S2 in the Supplementary Material). The degree of dissociation of each amino acid AA_k as a function of its $pK_a^{(k)}$ and pH is then given by the Henderson-Hasselbach equation:

$$q_k^+ = \frac{1}{1 + 10^{-pK_a^{(k)} + pH}} \quad \text{and} \quad q_k^- = -\frac{1}{1 + 10^{pK_a^{(k)} - pH}} \quad (2)$$

for bases ($q_k^+ > 0$) and acids ($q_k^- < 0$), respectively.

Cysteine protonation

Cysteine has a thiol functional end group which is a very weak acid; in addition, it is reactive and can form disulfide bonds. For these reasons it is often not considered as an acid at all: We will treat this by separately considering two cases where we either (i) do not take cysteine protonation into account, or (ii) consider the acidity of cysteine. Cysteine residues comprise between 2-14% of our studied proteins' AA composition at the RSA cut-off of $c = 0.25$ (cf. also Table S1). Due to its pK_a value (Table S2), cysteine's region of influence is limited to $pH > 7$ and its presence shifts charge distributions towards more negative values in that range [19]. For the most part we will not consider cysteine acidity in our analysis, and specifically point out the differences in the results we obtain when cysteine acidity is taken into account in the Discussion and Supplementary Material.

Surface charge distribution and electrostatic multipoles

With the approach outlined in the previous Subsections we can obtain, at any value of pH , the positions of charged residues for a given protein, $\mathbf{r}_k = (x_k, y_k, z_k)$, and the (fractional) charge they carry, q_k . To obtain a surface charge distribution we then project them onto a spherical surface, $\mathbf{r}_k = (R, \Omega_k) = (R, \vartheta_k, \varphi_k)$, so that their positions are characterized only by their solid angle, Ω_k . Here, the radius of the projecting sphere, R , can be any characteristic dimension of the protein, its circumscribed radius most often being used for this purpose [24].

The surface charge distribution of the discrete charges can then be written simply as

$$\begin{aligned} \sigma(\Omega) &= \frac{1}{4\pi R^2} \sum_{k \in AA} q_k \delta(\Omega_k) \\ &= \frac{1}{4\pi R^2} \sum_{l=0}^{\infty} \sum_{m=-l}^l \sigma_{lm} Y_{lm}(\Omega), \end{aligned} \quad (3)$$

if rewritten in the form of an expansion in terms of the irreducible spherical representation of multipoles; $\delta(x)$ is the Dirac delta function and $Y_{lm}(\Omega)$ are the spherical harmonics. From eq. (3) we can then obtain the *multipole expansion coefficients* σ_{lm} as

$$\sigma_{lm} = \sum_{k \in AA} q_k Y_{lm}^*(\Omega_k). \quad (4)$$

Since the original surface charge distribution consists of discrete charges (their positions being delta functions in the solid angle), we need in principle an infinite sum over l to obtain the exact multipole expansion of the original distribution. However, in absence of any symmetries of higher order (e.g., octahedral or icosahedral), the lower-order multipoles provide a good signature of the charge distributions in various molecules, and even a small number of higher-order multipoles can account for almost all of the electrostatic field [23, 24, 31–33].

In this work, we will thus mainly focus on the three lowest-order multipoles, the total charge (monopole with rank $\ell = 0$), the dipole moment ($\ell = 1$), and the quadrupole moment ($\ell = 2$). The total charge is independent of the choice of coordinates and can be obtained simply as

$$q = \sum_{k \in AA} q_k, \quad (5)$$

where k runs over all of the charged amino acids in the protein.

For simplicity, in dealing with the dipole and quadrupole moment we will rescale all our calculations with the characteristic radius of the protein R , thus effectively dealing with a unit sphere. The positions of the charges become unit vectors \mathbf{n}_k , expressed in spherical coordinates as $\mathbf{n}_k = (1, \vartheta_k, \varphi_k)$. As we will also be interested in the orientation of the dipole vector and the eigenvectors of the quadrupole tensor, it will be easier for us to deal with them in Cartesian coordinates. The expressions for the dipole vector $\boldsymbol{\mu}$ and the quadrupole tensor \mathcal{Q} are then [56]

$$\boldsymbol{\mu} = \sum_{k \in \text{AA}} q_k \mathbf{n}_k, \quad (6)$$

$$\mathcal{Q} = \frac{1}{2} \sum_{k \in \text{AA}} q_k (3\mathbf{n}_k \mathbf{n}_k - \mathbf{1}), \quad (7)$$

or in an obvious component notation (μ_i and Q_{ij}) that we do not write down explicitly. The proper units for the multipoles can be obtained by multiplying the expressions in eqs. (6) and (7) with the corresponding power of the characteristic protein radius R^ℓ (i.e., $\ell = 1$ for the dipole and $\ell = 2$ for the quadrupole). Cartesian components of both dipole and quadrupole moments can also be very easily transformed into a spherical form, in which they might be more suitable for analytical or numerical calculations (cf. Ref. [56]).

We choose the center-of-mass of each protein for the origin of the coordinate system in which we compute the surface charge distribution and the electrostatic multipoles. Since the monopole moment (the total charge) of the surface charge distribution is always non-zero except at the isoelectric point, the higher multipoles are dependent on the choice of the origin. However, the transformations of the dipole and quadrupole moment to other coordinate systems are very simple and given in Ref. [56].

Dipole and quadrupole principal axes

Surface charge distributions on the proteins, and therefore their multipole expansions, will change with pH . This will influence not only the magnitudes of the individual multipoles, but also their orientation in space. Consequently, we will be interested in the orientations of the dipole and quadrupole distributions with respect to the original (reference) coordinate system. For each protein, this coordinate system is derived from its PDB entry; the exact orientation of the original coordinate system compared to the protein structure will not be of interest to us, since we will be interested in relative changes of the dipole and quadrupole orientations with pH .

While the monopole moment is rotationally invariant, we can always find a rotation of the original coordinate system so that either (i) the dipole vector has a non-zero component only in the z direction, or (ii) the quadrupole tensor is diagonal, with the largest eigenvalue aligned along the z axis. We will refer to these two z axes in the rotated coordinate systems as the *dipole and quadrupole principal z axes*, respectively.

The dipole moment, being a vector, has three independent components: in the original coordinate system they are the $\mu_{x'}$, $\mu_{y'}$, and $\mu_{z'}$. Upon rotation into the dipole coordinate system, the dipole moment has a non-zero component only along its principal z axis, $\boldsymbol{\mu} = (0, 0, \mu_z)$, where $\mu_z = (\mu_{x'}^2 + \mu_{y'}^2 + \mu_{z'}^2)^{1/2}$. The two remaining parameters are now the two angles needed to align the original z' axis into the new, principal z axis. (Since the only non-zero component is in the z direction, the position of the new x and y axes is irrelevant.)

The quadrupole moment is a symmetric tensor, thus having five independent components. In the quadrupole coordinate system specified by its eigenvectors the tensor becomes diagonal, and we can always order its eigenvalues by value so that the largest one is oriented along the principal z axis, $Q_{xx} \leq Q_{yy} \leq Q_{zz}$. Since the quadrupole tensor is traceless, we can also express one of its eigenvalues with the other two, e.g., $Q_{yy} = -(Q_{xx} + Q_{zz})$. This leaves us with three more independent components which we can identify with, for instance, the three Euler angles needed to rotate the original coordinate system into the one defined by the quadrupole eigenvectors. Due to the symmetry of the quadrupole, we will also restrict the location of its principal z axis only to the upper hemisphere of the circumscribed sphere.

Quadrupole ratio

In the case of the quadrupole moment we will also be interested in the projections of the surface charge distributions along the y and x axes in the quadrupole coordinate system. Because of our choice of the ordering of the eigenvalues, Q_{zz} will always take on the largest positive value and Q_{xx} the largest negative value. Thus, a ratio of these two eigenvalues, $|Q_{xx}/Q_{zz}|$, will provide us with information on what proportion of the quadrupole distribution is aligned with the principal z and x axis, respectively. (The y axis information can be again omitted due to $\text{Tr}\mathcal{Q} = 0$.)

When the quadrupole ratio is close to 0.5, the quadrupole distribution is axial and oriented predominantly along the z axis. Likewise, when the ratio is close to 2.0, the distribution is axial but with an opposite sign and oriented along the x axis. On the other hand, when this ratio is close to 1, the distribution is represented symmetrically in the z and x directions while vanishing along the y axis. In this scenario, the distribution is not axial but corresponds better to a planar one. The ratio of the two quadrupole eigenvalues thus gives us an insight into the spatial distribution of the quadrupole, which can have an impact on, for instance, the interaction and assembly of molecules with a pronounced quadrupole moment. Some examples of the relation between the quadrupole ratio and the spatial distribution of the quadrupole moment are shown in Figs. S1 and S2 in the Supplementary Material.

RESULTS

pH dependence of multipole magnitudes

Before we focus on the spatial distribution of the multipole moments, we first observe how the value of pH influences their magnitude. In general, the total magnitudes of higher-order multipoles ($\ell \gtrsim 10$) are comparable to the lowest-order ones (see Fig. S3 in the Supplementary Material). This is understandable, as we are performing a multipole expansion of a set of Dirac delta functions which require an infinite sum to be reproduced exactly. However, as already described in the Materials and Methods section, higher-order multipoles are usually needed to describe details of charge distributions while their coarse-grained properties can be well characterized by the multipoles of lower order. In view of this, we will focus here only on the three lowest-order multipoles: the total charge, dipole moment, and quadrupole moment.

Figure 2 shows the pH dependence of the first three multipole components in the cases of lysozyme and HSA; similar plots for the MS2 capsid protein and β -lactoglobulin are shown in Fig. S4 in the Supplementary Material. The total charge on the proteins decreases from positive to negative as the pH increases, crossing the point of zero charge at the isoelectric point, pI . The isoelectric points of the proteins are interesting from the standpoint that, since the monopole moment vanishes, higher-order multipoles take on a greater importance. When cysteine acidity is not considered, the predicted isoelectric point of lysozyme is $pI = 11.08$, an alkaline pI that is in very good agreement with the values found in the literature ($pI \gtrsim 11$ [57, 58]), even though we used a fairly simple method to obtain it. The pI values we obtain for other proteins are listed in Table I and also correspond well with the experimental values: $pI = 4.7$ – 5.6 for HSA [59, 60] and $pI \sim 5.1$ for β -lactoglobulin [61, 62]. The pI value obtained for the phage MS2 capsid protein at a first glance disagrees with the very low reported value of the phage MS2, $pI \sim 2.2$ – 3.9 [63, 64]. The notable discrepancy stems most probably from the presence of the genome in the interior of the virion and the permeability of the capsid to external flow [65] – in studies where the capsid protein alone was considered, the obtained isoelectric point was at a $pI > 8$ [66–68]. Our results thus match the ones found in the literature, as we consider only a single capsid protein and not the formed virion (with or without the genome), even though they do not match the experimental results for the formed phage.

In contrast to the total charge, the dipole moment does not change its sign, which is expected, as we always orient the dipole coordinate system so that it points in the z direction. The pH dependence of the dipole magnitude

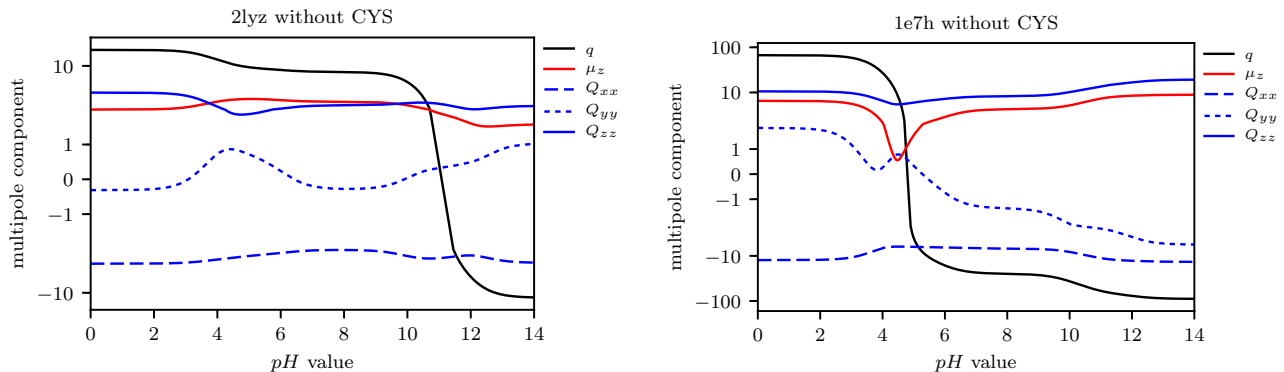


Figure 2. Magnitudes of the monopole (q), dipole (μ_z), and quadrupole (Q_{ii}) components of the surface charge distributions of lysozyme (2lyz) and human serum albumin (1e7h), shown as a function of pH . Cysteine acidity is not considered.

PDB	CYS	pI	$q_{\text{ext}} [e_0]$	pH_q	$\mu_{\text{max}} [e_0/R]$	pH_μ	$Q_{\text{max}} [e_0/R^2]$	pH_Q	$\langle Q_{xx}/Q_{zz} \rangle_{pH}$
2lyz	no	11.08	18.00	0.00	2.97	5.10	4.89	14.00	1.09
1e7h	no	4.78	-89.73	14.00	8.90	14.00	20.80	14.00	0.93
2ms2	no	9.78	-11.95	14.00	4.39	6.95	5.33	0.00	1.02
2blg	no	4.47	-26.97	14.00	7.11	8.00	4.60	14.00	0.91
2lyz	yes	10.53	18.00	0.00	2.97	5.10	6.74	14.00	1.24
1e7h	yes	4.78	-114.73	14.00	10.27	14.00	24.41	14.00	0.95
2ms2	yes	8.88	-13.95	14.00	4.39	5.75	6.11	14.00	1.07
2blg	yes	4.47	-27.97	14.00	7.85	9.00	4.36	13.50	0.97

Table I. Summary of results for the pH dependence of the magnitudes of multipole components, both when cysteine acidity is or is not considered. Listed are the extremum of the total charge and the maximum values of the dipole and quadrupole magnitudes [eq. (S1)] across the pH range, and the pH values where the maxima are attained. In addition we list the isoelectric point, pI , where the monopole moment (total charge) reaches zero, and the average of the quadrupole ratio $\langle |Q_{xx}/Q_{zz}| \rangle_{pH}$ across the range of pH values.

is nonetheless non-monotonic. In a similar fashion, the quadrupole components vary non-monotonically across the range of pH values, with the Q_{zz} and Q_{xx} values always being positive and negative, respectively, due to our definition of their direction. The value of Q_{yy} , as a consequence of $\text{Tr}Q = 0$, crosses zero when the Q_{xx} component becomes larger than the Q_{zz} component, or vice versa.

In order to be able to compare the different proteins between each other, we also list in Table I the maximum values of their multipole magnitudes [eq. (S1) in the Supplementary Material] across the entire range of pH values. All the proteins attain the extremum of charge and quadrupole magnitude at the either end of the pH interval; the difference here is that while the total charge changes monotonically with pH , the quadrupole moment shows quite a variation across the same range. The dipole moment, on the other hand, reaches its maximum magnitude usually somewhere in the mid-range of the pH values, with the exception of HSA, where all the moments are maximal at $pH = 14$. While the extremum of the total charge is always larger than the dipole and quadrupole maxima, the latter two are usually quite comparable. The proteins nonetheless exhibit certain differences in this aspect, too, as the maximum quadrupole moment of HSA is twice as large as its dipole moment, while the opposite is true in the case of β -lactoglobulin.

Quadrupole ratio: axial or planar distribution

We have seen that both Q_{zz} and Q_{xx} components of the quadrupole tensor exhibit non-monotonic variation with pH . To be able to interpret their relationship more easily we also plot their ratio, $|Q_{xx}/Q_{zz}|$, as a function of pH (Fig. 3). When either of the two components dominates, we have $|Q_{xx}/Q_{zz}| \sim 0.5$ or $|Q_{xx}/Q_{zz}| \sim 2.0$, and the distribution is axial along the z or x axis, respectively. On the other hand, when the two components are comparable,

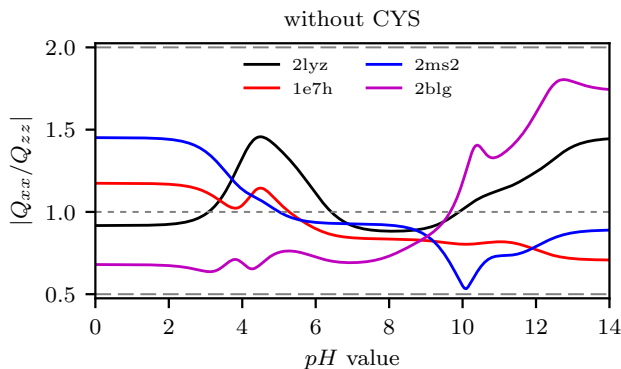


Figure 3. Quadrupole ratio $|Q_{xx}/Q_{zz}|$ as a function of pH for all the proteins studied; cysteine acidity is not considered. The ratio determines whether the quadrupole distribution is axial ($|Q_{xx}/Q_{zz}| = 0.5$ and $|Q_{xx}/Q_{zz}| = 2.0$), planar ($|Q_{xx}/Q_{zz}| = 1$), or somewhere in-between. For additional geometrical interpretation of the quadrupole ratio see Figs. S1 and S2.

we have $|Q_{xx}/Q_{zz}| \sim 1$, and the distribution is “planar” in the x - z plane. In all the cases studied the quadrupole ratio varies quite a lot, although for most proteins (with the exception of β -lactoglobulin) it never reaches a fully axial distribution. Conversely, in certain ranges of pH values the quadrupole distributions of all the proteins are approximately planar. This is also mirrored by the average values of their quadrupole ratios, which are indeed close to 1 (Table I).

These results indicate that the nature of quadrupole distributions in the proteins used in our work can be influenced by changing the pH : At certain values of pH , the quadrupole distributions are axial and thus oriented along a single axis (here, due to our definitions, along the z or x axis). At other values of pH , however, the quadrupole distribution becomes planar and symmetrically distributed in the x - z plane. The nature of the quadrupole distribution can thus change quite drastically with pH even without any concomitant changes in the conformation of the protein, which should influence, for instance, the interaction properties of these proteins.

pH dependence of dipole and quadrupole principal axes

Now that we have seen how the magnitudes of different multipole moments change with pH , we turn our attention to the pH dependence of the orientation of the dipole and quadrupole principal axes compared to the original (reference) coordinate system. Firstly, we show in Figs. 4a and 4b multipole expansions of the surface charge distribution of β -lactoglobulin with maximum ranks of $\ell = 6$ and $\ell = 2$, respectively. Separately, we also show in Figs. 4c and 4d both the dipole and quadrupole distributions in the original coordinate system. All the plots are shown at $pH = 7$, and a similar figure for HSA is shown in Fig. S5 in the Supplementary Material.

From the multipole representation of the surface charge distribution where terms up to $\ell = 6$ are included (Fig. 4a)

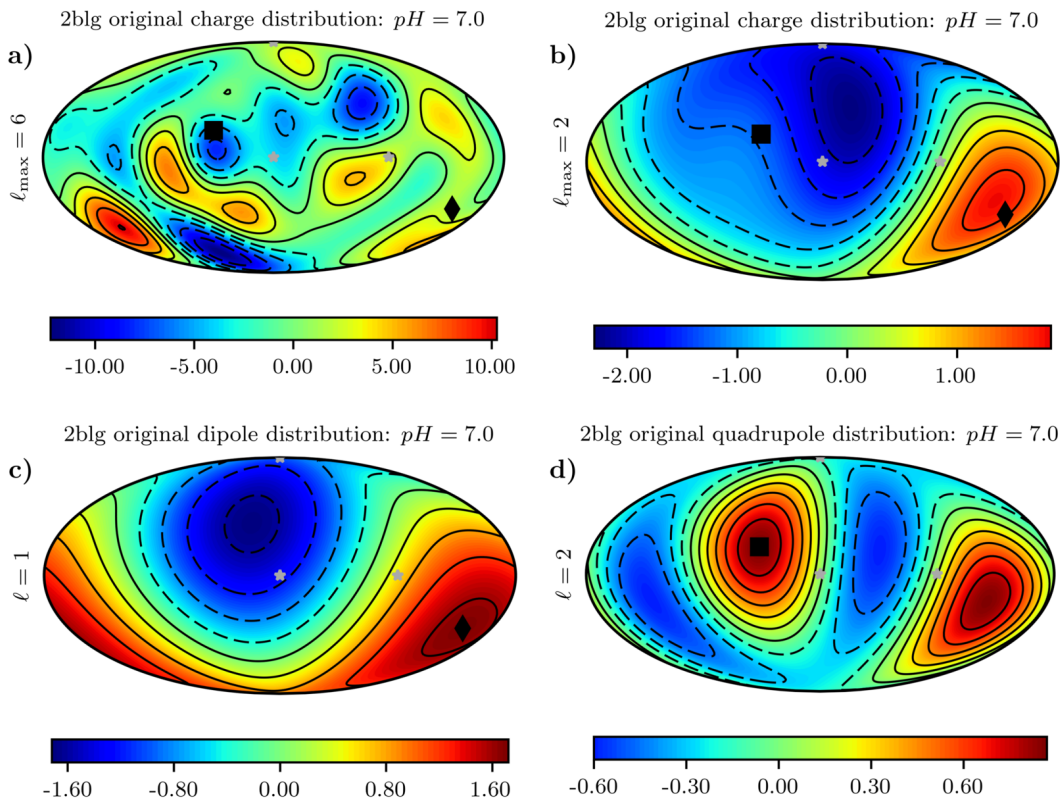


Figure 4. Multipole expansion of the surface charge distribution of β -lactoglobulin (2blg) in the original coordinate system up to (a) $\ell_{\max} = 6$ and (b) $\ell_{\max} = 2$. Shown are also the (c) dipole and (d) quadrupole distributions in the original (reference) system. The distributions are mapped from a sphere to a plane using the Mollweide projection. Black diamonds show the orientation of the z axis of the dipole, and black squares the orientation of the z axis of the quadrupole. Gray stars show the coordinate axes of the original coordinate system. Cysteine acidity is not considered, and all the plots are drawn at $pH = 7.0$.

it is not immediately obvious where the dipole and quadrupole axes are located. However, when we isolate both terms (Figs. 4c and 4d), this becomes more apparent. When the two distributions are combined together with the total charge (Fig. 4b), they describe the coarse-grained variation of the surface charge, even though they obviously cannot capture the patches of charge on smaller scales. Similar observations can be drawn also for the other proteins studied. For example, by comparing Figs. 4 and S5 we can observe a noticeable difference between β -lactoglobulin and HSA: In the former, the dipole distribution is the dominant among the lower-order multipoles, while the exact opposite is true in the case of the latter.

To demonstrate next how the orientations of the principal z axes of the dipole and quadrupole moments change with pH , we show in Fig. 5 snapshots of the multipole representation of the surface charge distribution of lysozyme (with $\ell_{\max} = 6$) at three different values of pH . Similar snapshots for HSA are shown in Fig. S6 in the Supplementary Material. For a complete comparison, Fig. 6 isolates the dipole and quadrupole principal z axes of all four proteins studied, and shows their variation in space over the entire range of pH values, with five positions of z axes at different values of pH isolated for illustration.

As pH is increased, the overall charge moves towards more negative values. At the same time, the positions of the dipole and quadrupole principal z axes trace quite a path in space. In the case of the lysozyme (Fig. 6a), most of the variation in the axes' orientation occurs after $pH > 7$. On the contrary, in the case of HSA (Fig. 6b) the majority of the variation, especially large in the case of the dipole, happens up until that point, i.e., when $pH < 7$. It is worth noting that the isoelectric points of the two proteins are at the opposite sides of the spectrum (Table I). The axes of the MS2 capsid protein exhibit perhaps the least variation (Fig. 6c), while the quadrupole axis of the β -lactoglobulin shifts in space to a large extent (Fig. 6d). (Note that the apparent jumps in the location of the quadrupole axis in the cases of HSA and β -lactoglobulin are a consequence of our confinement of the axis to the upper hemisphere for reasons of symmetry.)

Taken together, we see that not only does pH influence the magnitudes of the various multipole moments, but it influences even more so their orientation in space. The changes in the orientation do not happen uniformly with the changing pH , but are spaced unevenly across the range. Most of the variation usually (but not always) occurs in the pH range near the isoelectric point of each protein.

DISCUSSION

In a protein, the actual values of the acid-base dissociation constants pK_a are site-dependent, that is, influenced by the local ionic and structural environment [69, 70]. The deviations range from small to significant, depending on the type of site considered [8, 66]. While we did not consider the detailed structural environment in our work, we note that these changes effectively bring about a somewhat different configuration of charges on the surface of a protein, roughly similar to the effect the variation of the RSA cut-off c has on the surface charge distribution.

To show that the choice of the RSA cut-off does not have a large impact on the qualitative results of our study, we plot in Fig. S7 the pH dependence of the multipole moments of the four proteins studied for three different choices of the cut-off, ranging from $c = 0.1$ to $c = 0.5$. In each of the cases considered, going from $c = 0.1$ to $c = 0.5$ amounts to quite a significant loss of 24-34% of the total number of surface charges (see Table S1). And yet, some apparent

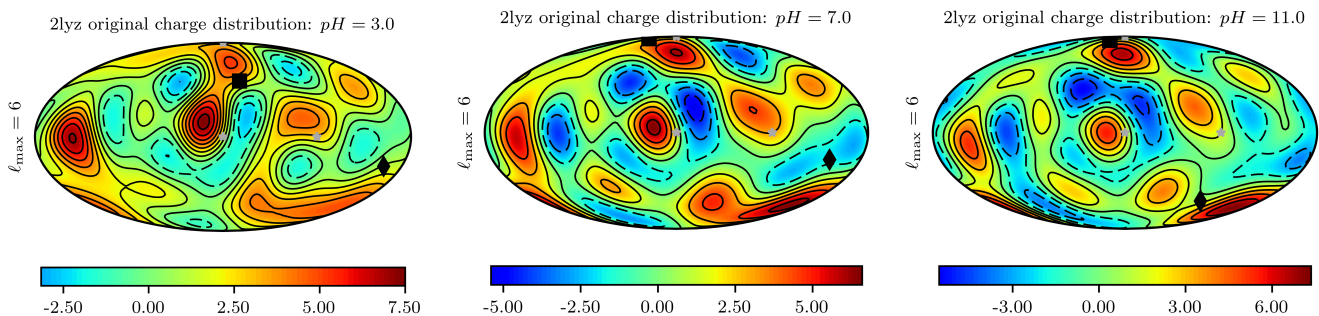


Figure 5. Multipole expansion of the surface charge distribution of lysozyme (2lyz) up to $\ell = 6$ in the original coordinate system, shown for three different values of $pH = 3, 7, 11$. The distributions are mapped from a sphere to a plane using the Mollweide projection. Black diamonds show the orientation of the z axis of the dipole, and black squares the orientation of the z axis of the quadrupole. Gray stars show the coordinate axes of the original coordinate system. Cysteine acidity is not considered.

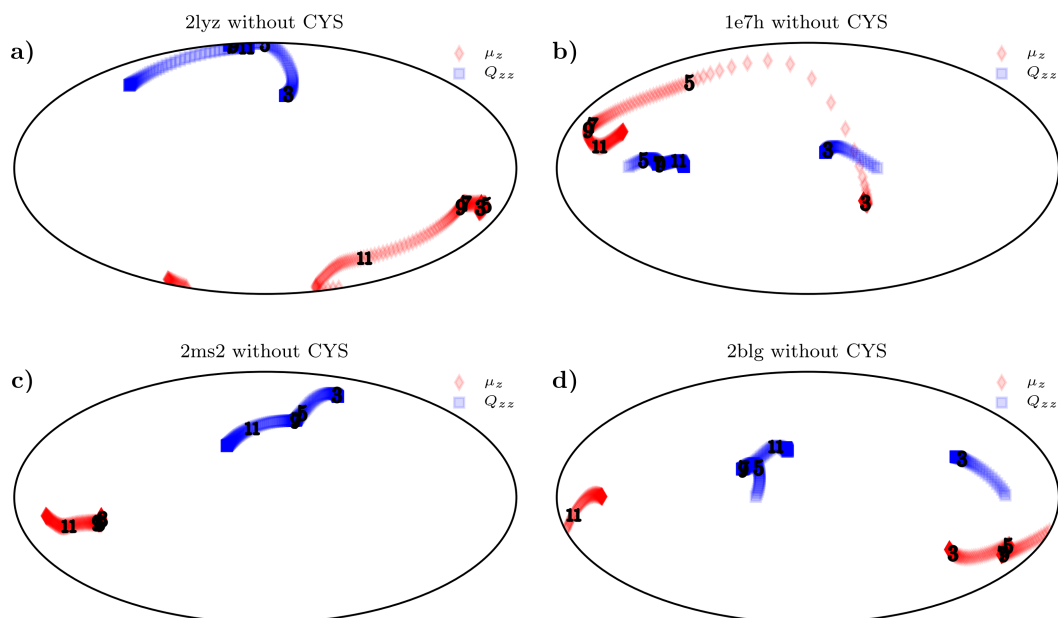


Figure 6. (a)-(d) Orientation of the dipole and quadrupole principal z axes (denoted by diamonds and squares, respectively) as a function of pH (in steps of $0.1 pH$ unit). The pH dependence of the axes' orientation is shown side by side for all four proteins included in our study. Individual numbers indicate the positions of both axes at five different pH values, $pH = 3, 5, 7, 9, 11$. The orientations of the axes are mapped from a sphere to a plane using the Mollweide projection. Cysteine acidity is not considered.

differences when the cut-off is increased notwithstanding, the qualitative behavior of the multipole moments remains much the same. This validates our approach, which fixed the cut-off to $c = 0.25$, and the conclusions drawn from it: While small variations of the number of charges on the surface of a protein will necessarily change the underlying multipole expansion of the surface charge distribution, the qualitative behavior we observed when the pH is varied will remain unaltered.

Allowing for the possibility of cysteine protonation should in principle have a similar effect (as the total number of charges increases), pushing the charge distribution towards more negative values at $pH > 7$. In order to see how the consideration of cysteine acidity influences our results, we show in Fig. S8 in the Supplementary Material a comparison of the pH dependence of the multipole magnitudes in the case of HSA and MS2 capsid protein. We can again observe that the presence of cysteine protonation has no qualitative effect on the behavior of the system. It does affect the location of the isoelectric point to some extent (cf. Table I), although the difference is less than 1 unit of pH . Other than that, the magnitudes of the multipole components and their pH dependence remain relatively unchanged. Similarly, by comparing the orientations of the dipole and quadrupole axes between the cases where cysteine acidity is or is not considered (Figs. S9 and 6, respectively) we see that the presence of cysteine charges influences the orientational variation of the principal axes at $pH > 7$, as expected, although the changes are usually minor. Most noticeably, the presence of cysteine acidity increases the orientational variation of the β -lactoglobulin quadrupole axis (Fig. S9d), while the orientational variation of the lysozyme dipole axis decreases to some extent (Fig. S9a).

The small changes observed can be in part related to the proportion of cystein residues in the proteins we considered here. From Table S1 we can see that the three smallest proteins (lysozyme, β -lactoglobulin, and MS2 capsid protein) have 3, 1, and 2 cysteine residues at the RSA cut-off of $c = 0.25$, respectively. HSA has a higher number of cysteine residues (25), but they still make up less than 15% of its total number of charged surface residues. The effect of cysteine acidity would be perhaps more pronounced in proteins in which cysteine composes a larger proportion of their AA make-up, although we can see that the qualitative behavior should remain similar to the one we observe here.

CONCLUSIONS

In this work, we studied the effects of pH on the multipole moments of charges in proteins. We first obtained pH -dependent surface charge distributions of four globular proteins and expanded the distributions in terms of electrostatic multipoles. We have limited ourselves mostly to lower-order multipoles (the total charge and the dipole and quadrupole moments), and studied the effect of both their magnitudes and the orientations of their principal axes in space. The value of pH was shown to have a significant effect on both, particularly on the orientations of the multipoles, which sometimes changed to a large degree. This variation in the orientation of the multipole principal axes was found to be a non-uniform function of pH , spaced rather unevenly across the solid angle, with most of the changes occurring in the pH range near the isoelectric point of each protein.

We have also pointed out some limitations of our approach, most notably the difficulty of precisely determining the fractional charge of amino acid residues in a protein. However, we have shown that the qualitative conclusions derived in our paper hold fast when we vary the magnitudes and positions of surface charges, and should thus stay valid even when a more detailed picture becomes attainable. Expanding our analysis to higher-order multipoles would also provide additional information on the electrostatic behavior of proteins. Since the multipole expansion was derived from point charges, the magnitudes of higher-order multipoles indeed turned out to be of a similar magnitude as the lower-order ones. Nonetheless, the first three multipole moments can already provide an electrostatic signature of each protein, and could potentially be used to classify different protein types [32]. In addition, defining and tracking the “orientations” of higher-order multipoles would require significantly more work as the number of parameters would increase and thus make our analysis less clear.

The orientational variation of the multipole principal axes should remain of fundamental importance also when screened electrostatic interactions in the presence of ionic solution are taken into account. There, the multipole moments play a significantly different role compared to the case of pure Coulomb interactions, in the sense that the screened electrostatic potential retains the full directional dependence of all multipole moments even in the far-field [34–37].

The major lesson of our investigation is that the pH variation of the direction of the multipole principal axes can affect the orientational electrostatic interaction between proteins even in the absence of any conformational change (which would imply an orientational deformation of the protein). This pH variation is highly protein-specific and should be of particular importance in protein assemblies, e.g., in viral capsids, where pH could in this way drive symmetry transitions induced by local, orientationally-dependent electrostatic interactions.

SUPPORTING MATERIAL

Two tables, nine figures, and one equation of supporting material are available.

We thank S. Čopar, G. Posnjak, and I. Rapošová for helpful discussions and comments on the manuscript. A.L.B. and R.P. acknowledge the financial support from the Slovenian Research Agency (research core funding No. (P1-0055)).

-
- [1] Leckband, D., and J. Israelachvili, 2001. Intermolecular forces in biology. *Q. Rev. Biophys.* 34:105–267.
 - [2] Leckband, D., and S. Sivasankar, 1999. Forces controlling protein interactions: theory and experiment. *Colloids Surf. B: Biointerfaces* 14:83–97.
 - [3] Piazza, R., 2004. Protein interactions and association: an open challenge for colloid science. *Curr. Opin. Colloid Interface Sci.* 8:515–522.
 - [4] Simonson, T., 2003. Electrostatics and dynamics of proteins. *Rep. Prog. Phys.* 66:737–787.
 - [5] Woods, L., D. Dalvit, A. Tkatchenko, P. Rodriguez-Lopez, A. Rodriguez, and R. Podgornik, 2016. A Materials Perspective on Casimir and van der Waals Interactions. *Rev. Mod. Phys.* 88:045003.
 - [6] Perutz, M., 1978. Electrostatic Effects in Proteins. *Science* 201:1187–1191.
 - [7] Warshel, A., P. Sharma, M. Kato, and W. Parson, 2006. Modeling electrostatic effects in proteins. *Biochim. Biophys. Acta* 1764:1647–1676.
 - [8] Gitlin, I., J. D. Carbeck, and G. M. Whitesides, 2006. Why are proteins charged? Networks of charge-charge interactions in proteins measured by charge ladders and capillary electrophoresis. *Angew. Chem. Int. Ed.* 45:3022–3060.
 - [9] Nozaki, Y., and C. Tanford, 1967. Examination of titration behavior. *Methods Enzymol.* 11:715–734.
 - [10] Lund, M., and B. Jönsson, 2005. On the Charge Regulation of Proteins. *Biochemistry* 44:5722–5727.
 - [11] da Silva, F. L. B., M. Lund, B. Jönsson, and T. Åkesson, 2006. On the complexation of proteins and polyelectrolytes. *J. Phys. Chem. B* 110:4459–4464.
 - [12] Barroso da Silva, F. L., and B. Jönsson, 2009. Polyelectrolyte-protein complexation driven by charge regulation. *Soft Matter* 5:2862–2868.

- [13] Finkelstein, A., and O. Ptitsyn, 2016. Protein Physics: A Course of Lectures. 2nd edition. Academic Press.
- [14] Gong, H., G. Hocky, and F. KF, 2008. Influence of nonlinear electrostatics on transfer energies between liquid phases: charge burial is far less expensive than Born Model. *Proc. Natl. Acad. Sci. USA* 105:11146–11151.
- [15] Isom, D., C. Castaneda, B. Cannon, P. Velu, and B. García-Moreno, 2010. Charges in the hydrophobic interior of proteins. *Proc. Natl. Acad. Sci. USA* 107:16096–16100.
- [16] Jensen, J. H., 2008. Calculating pH and salt dependence of protein-protein binding. *Curr. Pharm. Biotechnol.* 9:96–102.
- [17] Markovich, T., D. Andelman, and R. Podgornik, 2016. Charge regulation: a generalized boundary condition? *Europhys. Letts.* 113:26004.
- [18] Longo, G., M. Olvera de la Cruz, and I. Szleifer, 2012. Molecular theory of weak polyelectrolyte thin films. *Soft Matter* 8:1344–1354.
- [19] Nap, R. J., A. Lošdorfer Božič, I. Szleifer, and R. Podgornik, 2014. The role of solution conditions in the bacteriophage PP7 capsid charge regulation. *Biophys. J.* 107:1970–1979.
- [20] Lee, L., D. Cole, C.-K. Skylaris, W. Jorgensen, and M. Payne, 2013. Polarized Protein-Specific Charges from Atoms-in-Molecule Electron Density Partitioning. *J. Chem. Theory Comput.* 9:2981–2991.
- [21] Adhikari, P., A. Wen, R. French, V. Parsegian, N. Steinmetz, R. Podgornik, and W.-Y. Ching, 2014. Electronic Structure, Dielectric Response, and Surface Charge Distribution of RGD (1FUV) Peptide. *Sci. Rep.* 4:5605.
- [22] Eifler, R., R. Podgornik, N. Steinmetz, R. French, V. Parsegian, and W.-Y. Ching, 2016. Charge distribution and hydrogen bonding of a collagen α 2-chain in dry, hydrated and protonated/deprotonated structural models. *Int. J. Quantum Chem.* 116:681–691.
- [23] Gramada, A., and P. E. Bourne, 2006. Multipolar representation of protein structure. *BMC Bioinformatics* 7:242.
- [24] Hoppe, T., 2013. A simplified representation of anisotropic charge distributions within proteins. *J. Chem. Phys.* 138:174110.
- [25] Paulini, R., K. Müller, and F. Diederich, 2005. Orthogonal Multipolar Interactions in Structural Chemistry and Biology. *Angew. Chem. Int. Ed.* 44:1788–1805.
- [26] Yuan, Y., M. Mills, and P. Popelier, 2014. Multipolar electrostatics based on the Kriging machine learning method: an application to serine. *J. Mol. Model* 20:2172.
- [27] Yuan, Y., M. Mills, and P. Popelier, 2014. Multipolar Electrostatics for Proteins: Atom-Atom Electrostatic Energies in Crambin. *J. Comput. Chem.* 35:343–359.
- [28] Fletcher, T. L., and P. L. Popelier, 2016. Multipolar Electrostatic Energy Prediction for all 20 Natural Amino Acids Using Kriging Machine Learning. *J. Chem. Theory Comput.* 12:2742–2751.
- [29] Postarnakevich, N., and R. Singh, 2009. Global-to-local Representation and Visualization of Molecular Surfaces Using Deformable Models. In Proceedings of the 2009 ACM Symposium on Applied Computing. ACM, New York, NY, USA, SAC '09, 782–787.
- [30] Arzenšek, D., D. Kuzman, and R. Podgornik, 2015. Hofmeister Effects in Monoclonal Antibody Solution Interactions. *J. Phys. Chem. B* 119:10375–10389.
- [31] Platt, D. E., and B. D. Silverman, 1996. Registration, orientation, and similarity of molecular electrostatic potentials through multipole matching. *J. Comput. Chem.* 17:358–366.
- [32] Nakamura, H., and A. Wada, 1985. Nature of the charge distribution in proteins. III. Electric multipole structures. *J. Phys. Soc. Jpn.* 54:4047–4052.
- [33] Kim, J. Y., S. H. Ahn, S. T. Kang, and B. J. Yoon, 2006. Electrophoretic mobility equation for protein with molecular shape and charge multipole effects. *J. Colloid Interf. Sci.* 299:486–492.
- [34] Rowan, D., J.-P. Hansen, and E. Trizac, 2000. Screened electrostatic interactions between clay platelets. *Mol. Phys.* 98:1369.
- [35] Kjellander, R., and R. Ramirez, 2008. Yukawa multipole electrostatics and nontrivial coupling between electrostatic and dispersion interactions in electrolytes. *J. Phys.: Condens. Matter* 20:494209.
- [36] Lošdorfer Božič, A., and R. Podgornik, 2013. Symmetry effects in electrostatic interactions between two arbitrarily charged shells in the Debye-Hückel approximation. *J. Chem. Phys.* 138:074902.
- [37] Kjellander, R., 2016. Nonlocal electrostatics in ionic liquids: The key to an understanding of the screening decay length and screened interactions. *J. Chem. Phys.* 145:124503.
- [38] Šiber, A., A. Lošdorfer Božič, and R. Podgornik, 2012. Energies and pressures in viruses: contribution of nonspecific electrostatic interactions. *Phys. Chem. Chem. Phys.* 14:3746–3765.
- [39] Hieronimus, R., S. Raschke, and A. Heuer, 2016. How to model the interaction of charged Janus particles. *J. Chem. Phys.* 145:064303.
- [40] Yigit, C., J. Heyda, and J. Dzubiella, 2015. Charged patchy particle models in explicit salt: ion distributions, electrostatic potentials, and effective interactions. *J. Chem. Phys.* 143:064904.
- [41] Yigit, C., J. Heyda, M. Ballauff, and J. Dzubiella, 2015. Like-charged protein-polyelectrolyte completion driven by charge patches. *J. Chem. Phys.* 143:064905.
- [42] Yigit, C., M. Kanduč, M. Ballauff, and J. Dzubiella, 2017. Interaction of Charged Patchy Protein Models with Like-Charged Polyelectrolyte Brushes. *Langmuir* 33:417–427.
- [43] Bianchi, E., R. Blaak, and C. N. Likos, 2011. Patchy colloids: state of the art and perspectives. *Phys. Chem. Chem. Phys.* 13:6397–6410.
- [44] Bianchi, E., C. N. Likos, and G. Kahl, 2014. Tunable assembly of heterogeneously charged colloids. *Nano Lett.* 14:3412–3418.
- [45] Stipsitz, M., G. Kahl, and E. Bianchi, 2015. Generalized inverse patchy colloid model. *J. Chem. Phys.* 143:114905.
- [46] Berman, H. M., J. Westbrook, Z. Feng, G. Gilliland, T. N. Bhat, H. Weissig, I. N. Shindyalov, and P. E. Bourne, 2000.

The Protein Data Bank. *Nucleic Acids Res.* 28:235–242.

- [47] Pettersen, E. F., T. D. Goddard, C. C. Huang, G. S. Couch, D. M. Greenblatt, E. C. Meng, and T. E. Ferrin, 2004. UCSF Chimera – a visualization system for exploratory research and analysis. *J. Comput. Chem.* 25:1605–1612.
- [48] Sanner, M. F., A. J. Olson, and J.-C. Spehner, 1996. Reduced surface: an efficient way to compute molecular surfaces. *Biopolymers* 38:305–320.
- [49] Bendell, C. J., S. Liu, T. Aumentado-Armstrong, B. Istrate, P. T. Cernek, S. Khan, S. Picioreanu, M. Zhao, and R. A. Murgita, 2014. Transient protein-protein interface prediction: datasets, features, algorithms, and the RAD-T predictor. *BMC Bioinformatics* 15:82.
- [50] Pollastri, G., P. Baldi, P. Fariselli, and R. Casadio, 2002. Prediction of coordination number and relative solvent accessibility in proteins. *Proteins: Struct., Funct., Bioinf.* 47:142–153.
- [51] Yuan, Z., K. Burrage, and J. S. Mattick, 2002. Prediction of protein solvent accessibility using support vector machines. *Proteins: Struct., Funct., Bioinf.* 48:566–570.
- [52] Chen, H., and H.-X. Zhou, 2005. Prediction of solvent accessibility and sites of deleterious mutations from protein sequence. *Nucleic Acids Res.* 33:3193–3199.
- [53] Wu, W., Z. Wang, P. Cong, and T. Li, 2017. Accurate prediction of protein relative solvent accessibility using a balanced model. *BioData Min.* 10:1.
- [54] Tien, M. Z., A. G. Meyer, D. K. Sydykova, S. J. Spielman, and C. O. Wilke, 2013. Maximum allowed solvent accessibilities of residues in proteins. *PLoS ONE* 8:e80635.
- [55] Haynes, W. M., editor, 2016. CRC Handbook of Chemistry and Physics. CRC Press, Boston, 97th edition.
- [56] Gray, C. G., and K. E. Gubbins, 1984. Theory of Molecular Fluids, Vol. 1: Fundamentals. International Series of Monographs on Chemistry, Vol. 9. Clarendon, Oxford.
- [57] Wetter, L. R., and H. F. Deutsch, 1951. Immunological studies on egg white proteins IV. Immunochemical and physical studies of lysozyme. *J. Biol. Chem.* 192:237–242.
- [58] Strang, R. H. C., 1984. Purification of egg-white lysozyme by ion-exchange chromatography. *Biochem. Educ.* 12:57–59.
- [59] Evenson, M. A., and H. F. Deutsch, 1978. Influence of fatty acids on the isoelectric point properties of human serum albumin. *Clin. Chim. Acta* 89:341–354.
- [60] Langer, K., S. Balthasar, V. Vogel, N. Dinauer, H. Von Briesen, and D. Schubert, 2003. Optimization of the preparation process for human serum albumin (HSA) nanoparticles. *Int. J. Pharm.* 257:169–180.
- [61] Majhi, P. R., R. R. Ganta, R. P. Vanam, E. Seyrek, K. Giger, and P. L. Dubin, 2006. Electrostatically driven protein aggregation: β -lactoglobulin at low ionic strength. *Langmuir* 22:9150–9159.
- [62] Mercadante, D., L. D. Melton, G. E. Norris, T. S. Loo, M. A. Williams, R. C. Dobson, and G. B. Jameson, 2012. Bovine β -lactoglobulin is dimeric under imitative physiological conditions: dissociation equilibrium and rate constants over the pH range of 2.5–7.5. *Biophys. J.* 103:303–312.
- [63] Michen, B., and T. Graule, 2010. Isoelectric points of viruses. *J. Appl. Microbiol.* 109:388–397.
- [64] Dika, C., J. F. Duval, G. Francius, A. Perrin, and C. Gantzer, 2015. Isoelectric point is an inadequate descriptor of MS2, Phi X 174 and PRD1 phages adhesion on abiotic surfaces. *J. Colloid Interf. Sci.* 446:327–334.
- [65] Dika, C., J. F. L. Duval, H. M. Ly-Chatain, C. Merlin, and C. Gantzer, 2011. Impact of internal RNA on aggregation and electrokinetics of viruses: comparison between MS2 phage and corresponding virus-like particles. *Appl. Environ. Microbiol.* 77:4939–4948.
- [66] Langlet, J., F. Gaboriaud, C. Gantzer, and J. F. Duval, 2008. Impact of chemical and structural anisotropy on the electrophoretic mobility of spherical soft multilayer particles: the case of bacteriophage MS2. *Biophys. J.* 94:3293–3312.
- [67] Penrod, S. L., T. M. Olson, and S. B. Grant, 1996. Deposition kinetics of two viruses in packed beds of quartz granular media. *Langmuir* 12:5576–5587.
- [68] Schaldach, C. M., W. L. Bourcier, H. F. Shaw, B. E. Viani, and W. D. Wilson, 2006. The influence of ionic strength on the interaction of viruses with charged surfaces under environmental conditions. *J. Colloid Interf. Sci.* 294:1–10.
- [69] Hass, M. A., and F. A. Mulder, 2015. Contemporary NMR Studies of Protein Electrostatics. *Annu. Rev. Biophys.* 44:53–75.
- [70] Schaefer, M., M. Sommer, and M. Karplus, 1997. pH-dependence of protein stability: absolute electrostatic free energy differences between conformations. *J. Phys. Chem. B* 101:1663–1683.

Supplementary Material: pH dependence of charge multipole moments in proteins

A. Lošdorfer Božič and R. Podgornik

NUMBER OF SURFACE CHARGES AS A FUNCTION OF RSA CUT-OFF

	0.1	0.2	0.25	0.3	0.4	0.5
2lyz (no CYS)	30	30	30	28	26	23
2lyz (with CYS)	34	33	33	31	27	24
1e7h (no CYS)	164	162	157	152	145	119
1e7h (with CYS)	192	188	182	173	162	127
2ms2 (no CYS)	23	23	22	22	19	17
2ms2 (with CYS)	25	25	24	24	21	19
2blg (no CYS)	50	49	46	45	42	36
2blg (with CYS)	51	50	47	46	43	37

Table S1. Number of charges present on the solvent-exposed surfaces of proteins used in our study as a function of the RSA cut-off c , with or without considering the cysteine (CYS) acidity. The number of charges present on the surface decreases with increasing cut-off. Outlined in bold is the cut-off of $c = 0.25$, used for the majority of the main paper.

ACID-BASE EQUILIBRIUM CONSTANTS

	ASP	GLU	TYR	ARG	HIS	LYS	CYS
pK_a	3.71	4.15	10.10	12.10	6.04	10.67	8.14

Table S2. Intrinsic pK_a values of amino acid functional groups in bulk dilute aqueous solutions. Values taken from Ref. [55].

GEOMETRICAL INTERPRETATION OF THE QUADRUPOLE EIGENVALUES RATIO

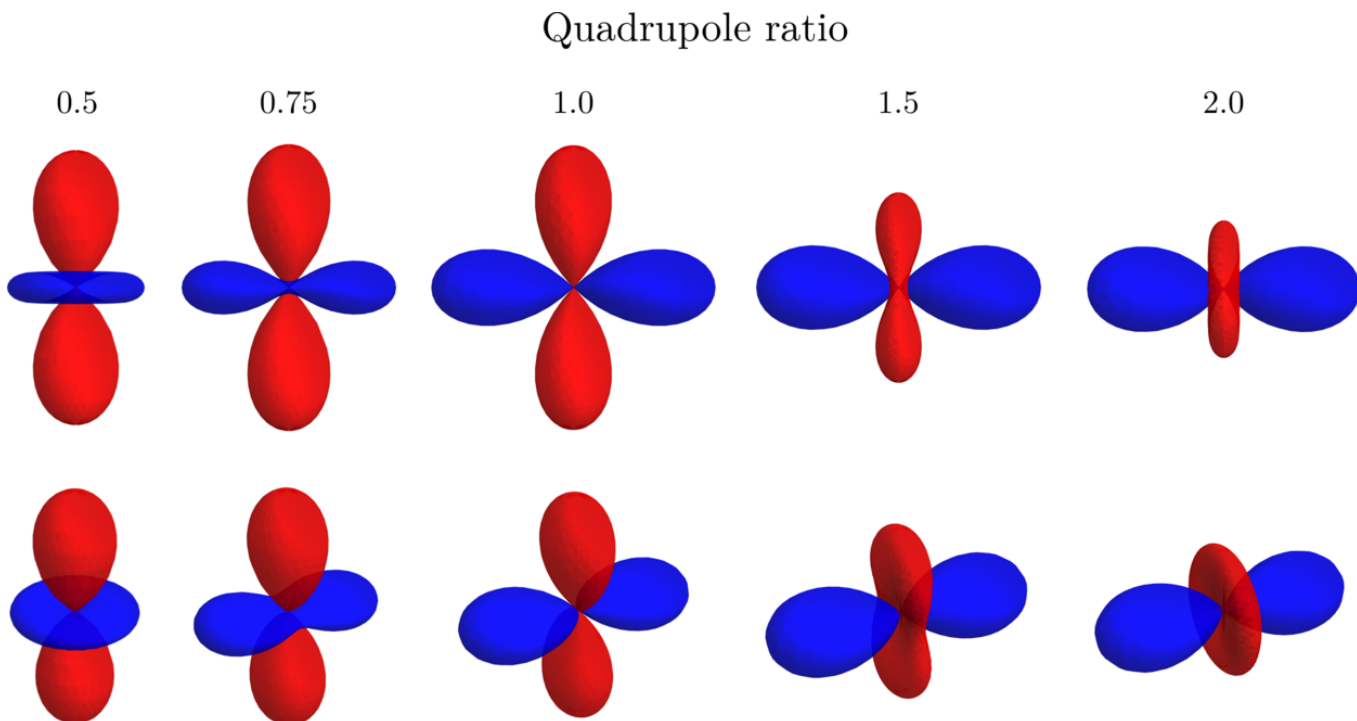


Figure S1. Illustration of quadrupole moment distributions for different values of the quadrupole ratio $|Q_{xx}/Q_{zz}|$ (0.5-2, left to right). The top and bottom rows show two different spatial perspectives of each ratio. Red color denotes positive values, blue negative, and the radius of the distribution corresponds to its magnitude. In the first of the extreme cases we have $|Q_{xx}/Q_{zz}| = 0.5$ and thus $Q_{xx} = Q_{yy}$. This corresponds to the case of an axial molecule, where the quadrupole is oriented along the z axis with a symmetric belt of opposite charge located in the x - y plane. A similar case is observed when $|Q_{xx}/Q_{zz}| = 2$ and the distribution is oriented along the x axis with $Q_{zz} = Q_{yy}$. In the other extreme, we have $|Q_{xx}/Q_{zz}| = 1$ and thus $Q_{xx} = -Q_{zz}$ with $Q_{yy} = 0$. In this case, the quadrupole distribution projected is symmetric in the x - z plane and vanishes completely along the y axis. See also Fig. S2 for some of these distributions projected onto a plane.

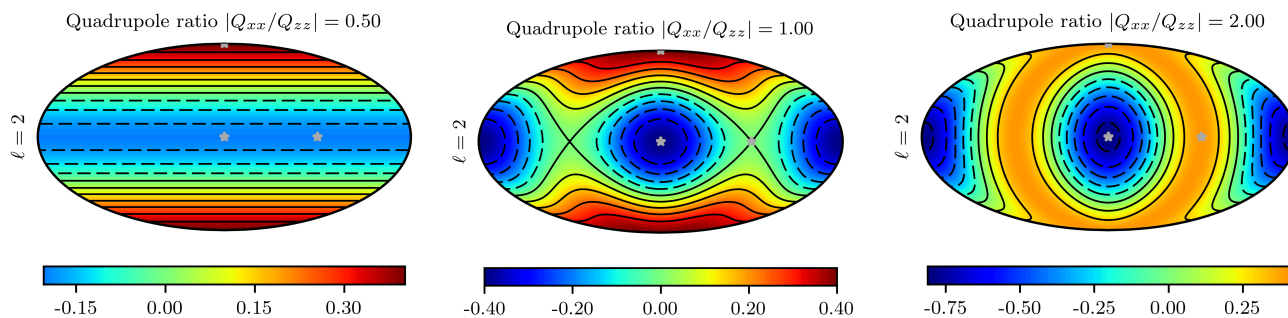


Figure S2. Quadrupole distributions with $Q_{zz} = 1$ and different values of the quadrupole ratio $|Q_{xx}/Q_{zz}|$. The distributions are mapped from a sphere to a plane using the Mollweide projection. The axes of the coordinate system are shown in gray. See Fig. S1 for details.

PH DEPENDENCE OF MULTIPOLE MAGNITUDES

To compare the multipoles between each other, we calculate their magnitude, S_ℓ , given in spherical coordinates as

$$S_\ell^2 = \frac{4\pi}{2\ell + 1} \sum_m |\sigma_{lm}|^2. \quad (\text{S1})$$

This multipole magnitude corresponds to the absolute value of the total charge for $\ell = 0$, the Cartesian norm of the dipole vector for $\ell = 1$, and to $S_2 = [(Q_{xx} - Q_{yy})^2 + Q_{zz}^2]^{1/2}$ in the case of the quadrupole, $\ell = 2$.

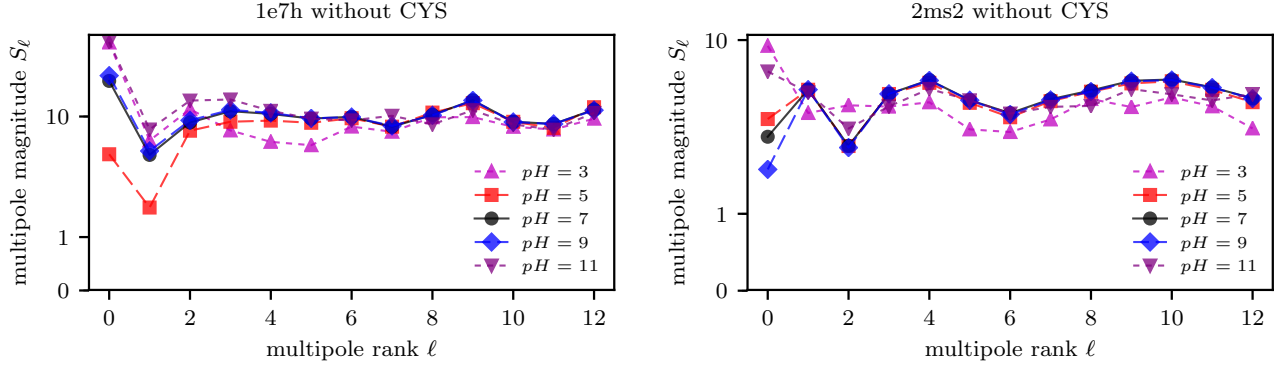


Figure S3. Magnitudes of multipole moments with rank $\ell = 0-12$, calculated from eq. (S1) and shown for 5 different values of pH . The plots show the magnitudes of the surface charge distributions of human serum albumin (1e7h) and MS2 capsid protein (2ms2). Cysteine acidity is not considered.

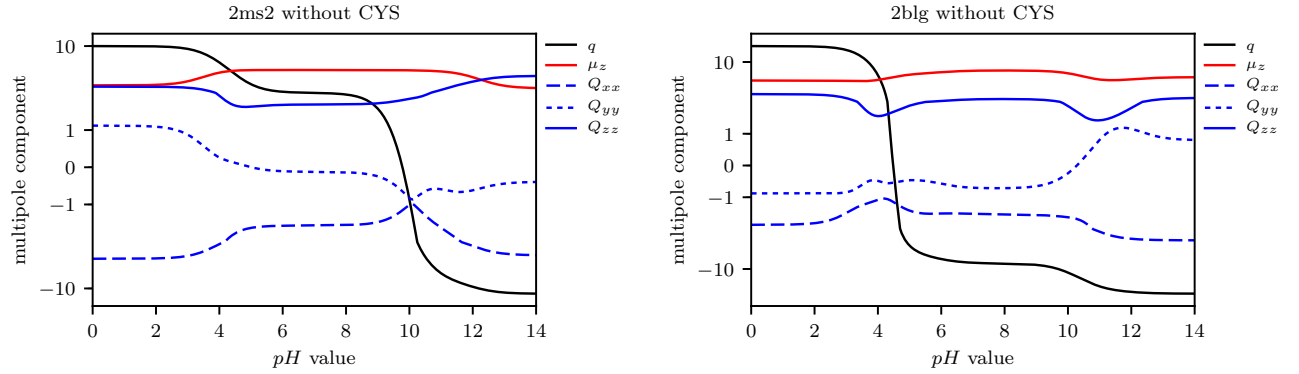


Figure S4. Magnitudes of the monopole (q), dipole (μ_z), and quadrupole (Q_{ii}) components of the surface charge distributions of the MS2 capsid protein (2ms2) and β -lactoglobulin (2blg), shown as a function of pH . Cysteine acidity is not considered.

PH DEPENDENCE OF DIPOLE AND QUADRUPOLE PRINCIPAL AXES

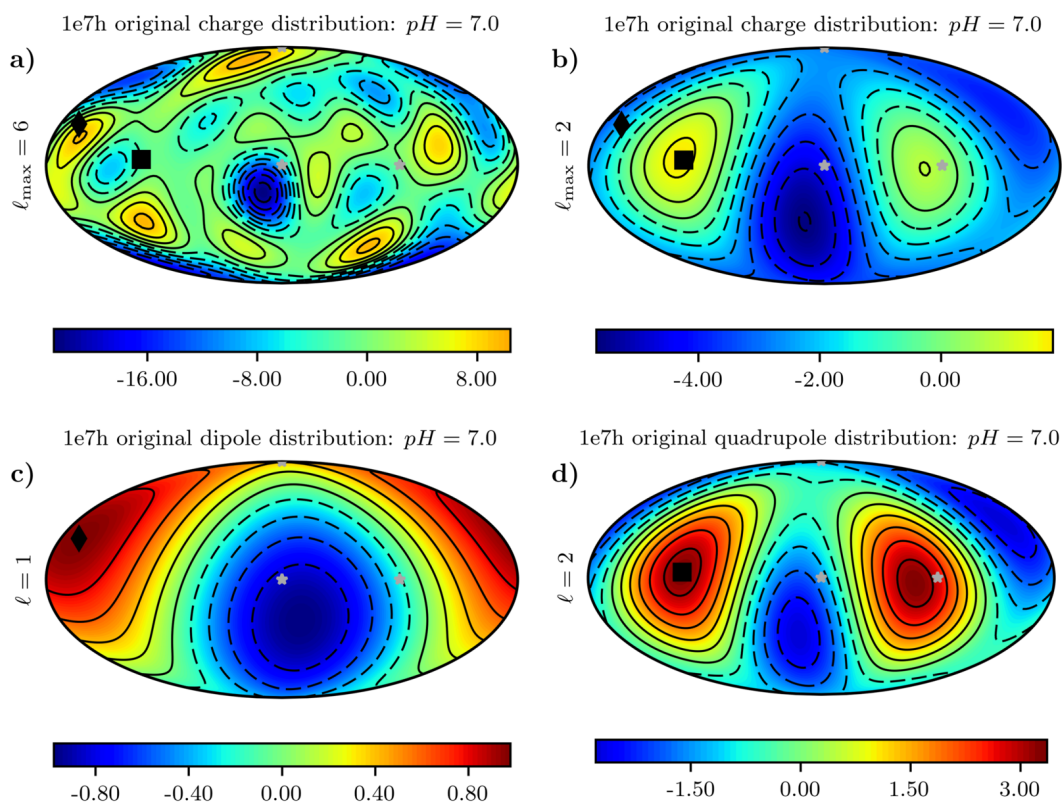


Figure S5. Multipole expansion of the surface charge distribution of human serum albumin (1e7h) in the original coordinate system up to (a) $\ell_{\max} = 6$ and (b) $\ell_{\max} = 2$. Shown are also the (c) dipole and (d) quadrupole distributions in the original (reference) system. The distributions are mapped from a sphere to a plane using the Mollweide projection. Black diamonds show the orientation of the z axis of the dipole, and black squares the orientation of the z axis of the quadrupole. Gray stars show the coordinate axes of the original coordinate system. Cysteine acidity is not considered, and all the plots are drawn at $pH = 7.0$.

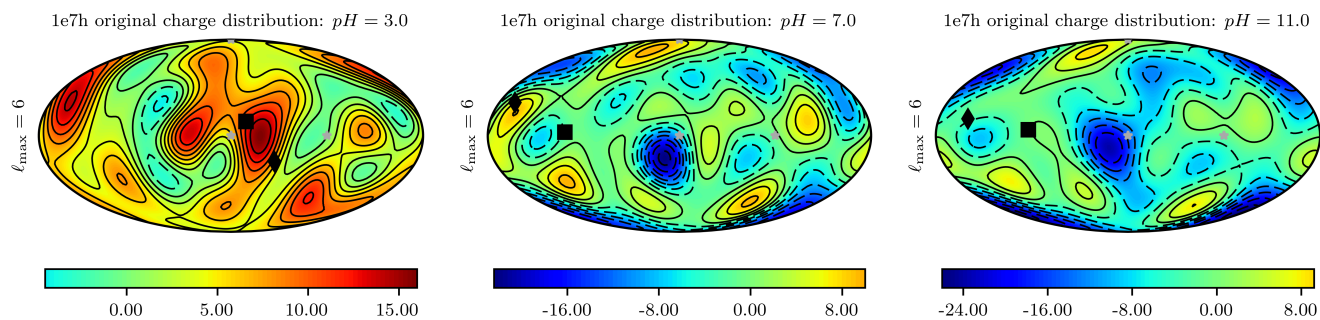


Figure S6. Multipole expansion of the surface charge distribution of human serum albumin (1e7h) up to $\ell = 6$ in the original coordinate system, shown for three different values of $pH = 3, 7, 11$. The distributions are mapped from a sphere to a plane using the Mollweide projection. Black diamonds show the orientation of the z axis of the dipole, and black squares show the orientation of the z axis of the quadrupole. Gray stars show the coordinate axes of the original coordinate system. Cysteine acidity is not considered.

RSA CUT-OFF VARIATION

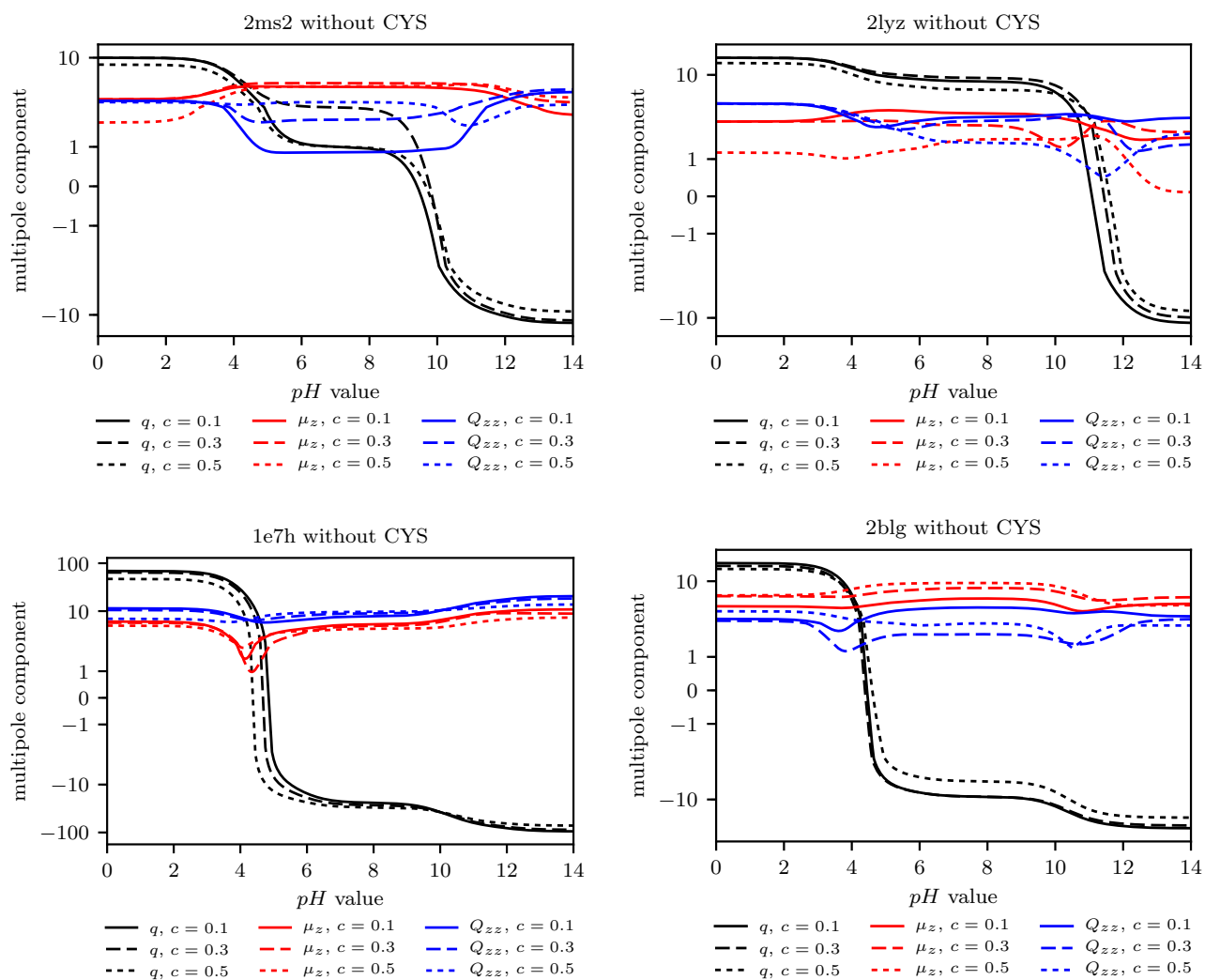


Figure S7. Multipole components as a function of pH for three different values of the RSA cut-off, $c = 0.1, 0.3, 0.5$. Shown for all four proteins: the MS2 capsid protein (2ms2), lysozyme (2lyz), human serum albumin (1e7h), and β -lactoglobulin (2blg). Cysteine acidity is not considered.

CYSTEINE PROTONATION

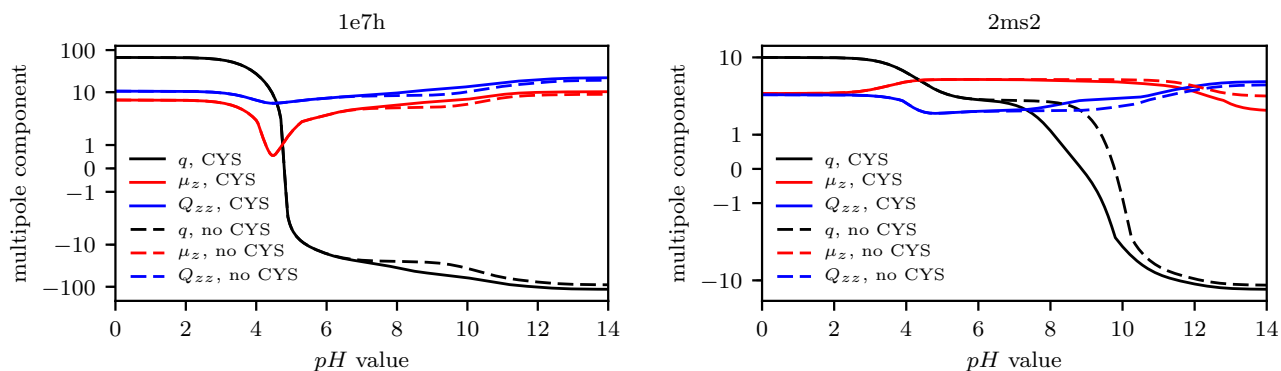


Figure S8. Comparison of the magnitudes of the monopole (q), dipole (μ_z), and quadrupole (Q_{ii}) components of the surface charge distribution as a function of pH between the cases where cysteine acidity is considered (full lines) or is not considered (dashed lines). Shown for human serum albumin (1e7h) and phage MS2 capsid protein (2ms2).

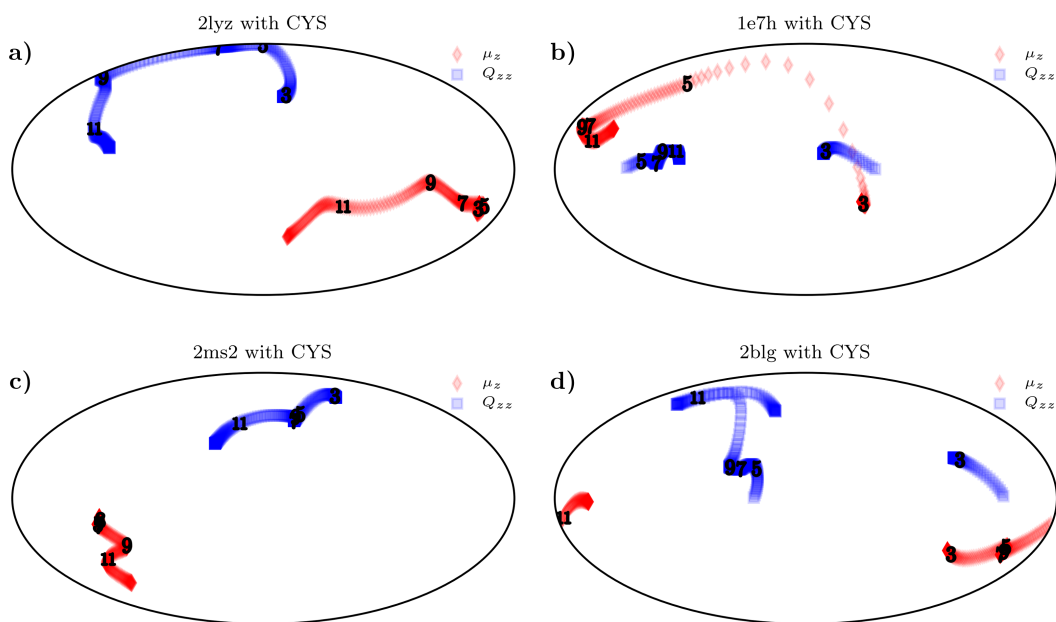


Figure S9. (a)-(d) Orientation of the dipole and quadrupole principal z axes (denoted by diamonds and squares, respectively) as a function of pH (in steps of $0.1 pH$ unit). The pH dependence of the axes' orientation is shown side by side for all four proteins included in our study. Individual numbers indicate the positions of both axes at five different pH values, $pH = 3, 5, 7, 9, 11$. The orientations of the axes are mapped from a sphere to a plane using the Mollweide projection. Cysteine acidity is considered; compare with Fig. 6 in the main text.